Radiation and Control of Sound from Evolving Wave Packet on a Concave-Convex Surface

Lucio Maestrello*
NASA Langley Research Center, Hampton, Virginia 23665
and
Nabil M. El-Hady†
Analytical Services and Materials, Inc., Hampton, Virginia 23665

Active control of the acoustic pressure in the far field resulting from the growth and decay of a wave packet convecting in a boundary layer over a concave-convex surface is investigated numerically using direct computations of the Navier-Stokes equations. The resulting sound radiation is computed using the linearized Euler equations with the pressure from the Navier-Stokes solution as a time-dependent boundary condition. The acoustic far field exhibits a directivity type of behavior that points upstream to the flow direction. A fixed control algorithm is used where the attenuation signal is synthesized by a filter that actively adapts itself to the amplitude-time response of the outgoing acoustic wave.

I. Introduction

THE objective of this paper is to investigate the acoustic field and the control of the acoustic radiation resulting from the evolution of a wave packet in an unstable boundary layer over a concave-convex curvature. An engineering application to this problem is the flow through a wind-tunnel contraction. The concave portion is known to be potentially unstable to upstream disturbances, whereas the convex portion is stabilizing. Both concave and convex portions are sources of sound radiation due to convective instability waves. This instability can be reduced by active surface heating. However, the intensity of the resulting sound may still be sufficient to trigger further instability, for example, on a model leading edge downstream. Therefore, control of sound radiation by virtual cancellation of the far-field pressure has to be dealt with.

In a wind-tunnel contraction, the disturbances entering the wall boundary layer may grow due to the unfavorable pressure gradient, a source of sound radiation, resulting in both standing and traveling waves. In addition, a patch of turbulence convecting through the pressure gradient created by the contraction geometry undergoes a variable rate of strain, thereby generating sound. The perturbation field from the boundary layer as well as from the sources embedded in the inviscid flow interacts with the leading edge of the model and is a possible source of transition.

The effect of surface curvature on time harmonic instability waves and active control of these waves by localized time-periodic surface heating has been considered previously by Maestrello et al.[1,2] Experimentally, active control using sound was shown by Dines,[3] Ffowcs Williams and Huang,[4] and Maestrello.[5] The mechanism of sound generation due to a wave packet propagating in viscous flow has been analyzed by Crighton and Huerre[6] and Haj-Hariri and Akylas.[7]

The present analysis is based on the numerical solution of the two-dimensional, laminar, Navier-Stokes equations where a fourth-order-accurate, operator-split algorithm is being used. An initial steady solution is obtained by imposing a steady boundary-layer solution at the inflow. An unsteady disturbance of finite duration is then introduced at the inflow in the form of a Tollmien-Schlichting wave and its subharmonic. Hence, a wave packet is created that grows and decays as it passes through the region of curvature-induced pressure gradient. The acoustic radiation resulting from the evolution of the wave packet is evaluated by solving the linearized Euler equations. The pressure computed from the Navier-Stokes equations is used as time-dependent boundary condition.

In this paper we deal with an unsteady, inhomogeneous flow problem, whose space-time complexity sets numerous limits and constraints on the technology needed for its control. We note that the control of the sound field is not conditional on the requirement to change the original source. However, active sound control can be accomplished by using the concept of antisound, as presented by Ffowcs Williams,[8] where the effects of sound and its directive interference artificially generated counterpart, the antisound, produce silence. Here, suppression of the acoustic field is achieved using a finite number of secondary acoustic sources in the far field appropriately programmed to cancel the outgoing pressure field.

In the following section we discuss the numerical algorithm, the determination of the acoustic field, and the principles of operation of a system for the implementation of the active sound control. In Sec. III, we present numerical results for both the uncontrolled and controlled acoustic field, followed by the concluding remarks in Sec. IV.

II. Analysis

Figure 1 shows the surface geometry and the domain used in the numerical computations. It consists of a concave-convex

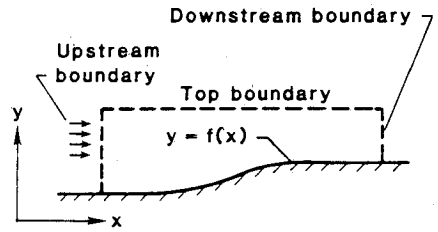

Fig. 1 Schematic of the surface geometry and computational domain.

Presented as Paper 89-1110 at the AIAA 12th Aeroacoustics Conference, San Antonio, TX, April 10-12, 1989, received July 26, 1989; revision received March 12, 1990; accepted July 24, 1990.

*Scientist, Acoustics Division. Associate Fellow AIAA.
†Senior Scientist, Fluid Mechanics Division. Senior Member AIAA.

surface with flat portions upstream and downstream with total length of 3.6 ft. The curved portion is described by a seventh-degree polynomial with the first three derivatives continuous at both ends.

A. Disturbance Field

The flowfield is governed by the two-dimensional, compressible, laminar Navier-Stokes equations. In Cartesian coordinates, x and y, these equations can be written in the conservative form

$$\boldsymbol{Q}_t = F_x + G_y \tag{1}$$

where $\boldsymbol{Q}$ is the vector $(\rho,\rho u,\rho v,e)^T$, ρ is the density, u and v are the x and y components of the velocity, respectively, and e is the total energy. The fluxes F and G are standard and will be omitted. System 1 is supplemented by the equation of state for an ideal gas $p = \rho RT$, where p is the pressure, T is the temperature, and R is the gas constant. The variation of the viscosity with the temperature $\mu(T)$ is governed by Sutherland's law.

The curved surface is assumed to be a single-valued function of x described by $y = f(x)$. In order to compute the flow over the curved surface, a general nonorthogonal coordinate transformation $\xi = \xi(x,y)$, and $\eta = \eta(x,y)$ is used and the transformed system is solved by an explicit finite-difference scheme on the rectangular grid (ξ,η) in the computational plane. Details of the specific coordinate transformation used are discussed in Ref. 1. The curvature is sufficiently mild that it is believed that no errors are introduced by the lack of orthogonality.

The finite-difference scheme used here is a modification of the MacCormack scheme, making it fourth-order accurate on the convective terms. The scheme is second-order accurate in time and on the viscous terms for nonconstant viscosity. The fourth-order accuracy is essential in order to prevent viscous-like truncation errors on the convective terms from artificially decreasing the effective Reynolds number of the computations and to prevent numerical dispersion and dissipation from altering the character of the waves that are computed in the mean flow.

The numerical scheme applied to the one-dimensional equation,

$$\boldsymbol{Q}_t = F_x$$

consists of predictor and corrector of the form

$$\bar{\boldsymbol{Q}}_i = \boldsymbol{Q}_i^n + \frac{\Delta t}{6\Delta x}(-7F_i + 8F_{i+1} - F_{i+2}) \tag{2a}$$

$$\boldsymbol{Q}_i^{n+1} = \frac{1}{2}\left\{\bar{\boldsymbol{Q}}_i + \boldsymbol{Q}_i^n + \frac{\Delta t}{6\Delta x}(7\bar{F}_i - 8\bar{F}_{i-1} + \bar{F}_{i-2})\right\} \tag{2b}$$

where the subscript i denotes the spatial grid point, and the superscript n denotes the time level. Scheme 2 becomes fourth order when alternated with a symmetric variant.

The two-dimensional problem is treated by operator splitting. Thus, if L_x denotes a solution operator symbolized by Eq. (2) for the equation $\boldsymbol{Q}_t = F_x$, and L_y denotes a similar operator for the equation $\boldsymbol{Q}_t = G_y$, then the solution to Eq. (1) is obtained by

$$\boldsymbol{q}^{n+2} = L_x L_y L_y L_x \boldsymbol{Q}^n \tag{3}$$

Split scheme (3) preserves the second-order accuracy in time and the fourth-order accuracy in space. This numerical scheme is applied to the transformed system and is described in detail by Bayliss et al.[9]

A steady solution is computed with a steady boundary-layer profile imposed at the inflow. Then, unsteady solutions are generated by modifying the inflow data in the form

$$\boldsymbol{Q}_{\text{inflow}} = \boldsymbol{Q}_0 + \epsilon\left[A_1 \text{Re}\{\zeta_1(y)e^{i\omega_1 t}\} + A_2 \text{Re}\{\zeta_2(y)e^{i\omega_2 t}\}\right]\kappa(t) \tag{4}$$

where $\boldsymbol{Q}_0$ is the computed steady state, ω_1 is a spatially unstable frequency, $\omega_2 = \omega_1/2$ is the subharmonic, ζ_1 and ζ_2 are the corresponding eigenfunctions of the compressible stability equations computed by El-Hady[10] for a given boundary-layer profile at the specified inflow Reynolds number, A_1 and A_2 are weighting constants, and ϵ is a parameter that determines the amplitude of the disturbance. The function $\kappa(t)$ is designed to create a pulse of finite duration and is defined as

$$\begin{aligned}\kappa(t) &= 0, \quad t \le 0\\ &= 0, \quad t \ge 2\pi/\omega_2\\ &= 0, \quad 0 \le t \le 2\pi/\omega_2\end{aligned} \tag{5}$$

In practice, $\kappa(t)$ is smoothed out near 0 and $2\pi/\omega_2$. It is found that acoustic waves are generated during the rise and decay of $\kappa(t)$.

The inflow boundary data are specified on the three incoming characteristics. Radiation boundary conditions are applied at the other boundaries. For a complete description of the boundary conditions, see Maestrello et al.[2]

B. Acoustic Field

Because of the vastly different length scales between the acoustic far field and the boundary layer, it is not feasible to compute the acoustic far field concurrently with the Navier-Stokes simulation. The acoustic analogy introduced by Lighthill[11] provides a formalism to couple a wave equation with the near-field behavior of the viscous flow to determine the acoustic far field. The Lighthill theory is generally computed by using the Green's function appropriate to the geometry and reducing the wave equation to an integral of the Lighthill sources against Green's function. Such a procedure was used analytically by Howe,[12] and Hardin and Lamkin.[13] The computations of Farassat[14] also used the Lighthill integral with the added complexity of noncompact sources.

The use of the Lighthill integral has several disadvantages for the problem considered here, especially when the integral becomes difficult to compute. The unsteady Navier-Stokes solution, which is basically a wave packet propagating over the curved surface, is the source that is radiating sound into the far field. The typical length scale in the streamwise direction is small compared with the acoustic wavelength for low Mach numbers; hence, the source region is considered to be acoustically compact. Our approach is to solve the linearized Euler equations using the pressure computed from the Navier-Stokes equations as time-dependent boundary data, as suggested in Ref. 7.

Specifically, we assume that the unsteady disturbances in the inviscid region satisfy the two-dimensional Euler equations linearized about a uniform flow with the prescribed freestream Mach number. We assume that the Mach number is small so that scattering of sound by the flow is neglected and that the inviscid disturbances are homentropic so that the fluctuating

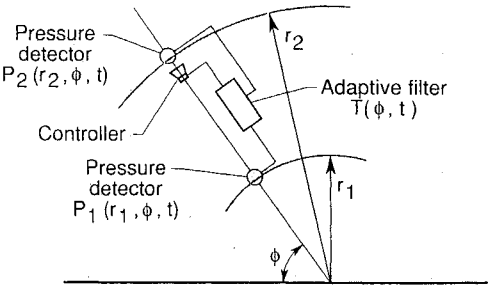

Fig. 2 Schematic of the sound control system.

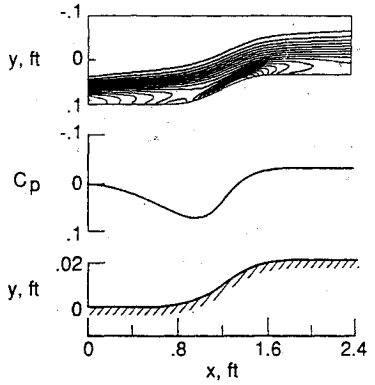

Fig. 3 Pressure distribution and mean vorticity; contours from 10-130(10).

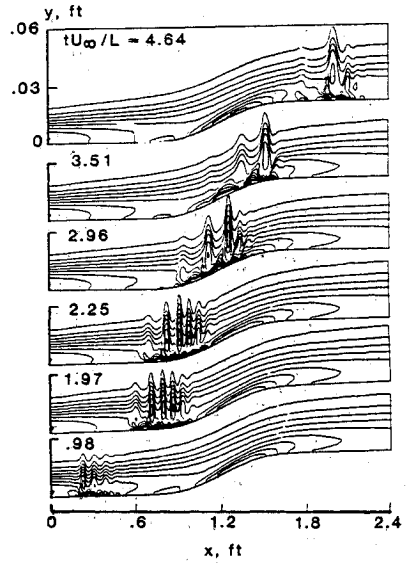

Fig. 4 Instantaneous total vorticity; contours from 10-130(10).

pressure can be related to the fluctuating density. The linearized system of equations in a nondimensional form is then

$$p_t + p_x + (u_x + v_y)/M_\infty^2 = 0 \tag{6a}$$

$$u_t + u_x + p_x = 0 \tag{6b}$$

$$v_t + v_x + p_y = 0 \tag{6c}$$

where p is the pressure, u and v are the streamwise and normal velocities, respectively, and M_∞ is the freestream Mach number.

For the inviscid calculations we assume that the curvature of the surface is negligible on the acoustic length scale and impose as a boundary condition at $y = 0$ the unsteady pressure computed from the Navier-Stokes equations, which is

$$p(x,0,t) = H(x,t) \tag{7}$$

At present, we have only imposed the pressure computed on the wall, although one could also justify imposing the pressure computed at the edge of the boundary layer.

The numerical computations of the linearized system (6) are performed using a scheme similar to that described earlier for the Navier-Stokes equations. The code is described by Bayliss et al.[15] and has been validated against a number of exact solutions. In order to eliminate reflections from the lateral boundaries, we use the method of Smith,[16] in which two solutions with acoustically hard and soft boundary conditions, respectively, are computed and averaged.

C. Active Sound Suppression

Attention is focused on the control of sound in the far-field spatial domain. The linearity of the acoustic field is an important desirable feature for dealing with the unsteady field. Active control of the linear acoustic field is accomplished by activating a secondary perturbation designed to destructively interfere with the outgoing wave field utilizing the principle of superposition.

The asymmetry of the radiating field due to the varying radiation rate of the sources as they convect about the curved surface makes the task of active cancellation more difficult than that for the sound generated by symmetric radiating sources. In this study the resulting sound radiation into the far field is highly directional, and the application of active cancellation requires different settings for the control system to attenuate the acoustic amplitude at different angles in the far field.

The control method adapted here is characterized as fixed control approach. A pressure signal $p_1(r_1,\phi,t)$ at a radius r_1 from the source over the concave-convex surface is used as a reference as well as input to a filter. The output function $T(\phi,t)$ from the filter is used as input to the controller (speaker). The controller is triggered by the arrival of another signal $p_2(r_2,\phi,t)$ at a farther radius r_2 along the same ray (see Fig. 2). The resulting interference of the two out-of-phase signals T and p_2 will produce an attenuated signal p_c at r_2. Figure 2 presents a simplified model of the sound control system at a fixed angle ϕ.

III. Results and Discussion

A. Flow Stability

All of the results presented are for an inflow Mach number of 0.4 and a unit Reynolds number (Re/ft) of 3×10^5 based on freestream values. The corresponding Reynolds number based on boundary-layer displacement thickness is 998.

Figure 3 shows the surface geometry together with the distribution of the pressure coefficient $C_p = (p - p_{\infty_i})/0.5\rho_{\infty_i}U_{\infty_i}^2$ and the mean vorticity contours. The subscripts ∞ and i refer to the freestream and the inflow conditions, respectively. The concave portion produces an adverse pressure gradient, whereas farther downstream the curvature becomes convex, resulting in a favorable pressure gradient. Because of the large velocity gradient on the curved portion, there is a concentration of vorticity. This portion, as will be seen later, plays an important role in the flow stability as well as in acoustic radiation.

We next consider the unsteady flow obtained by introducing a disturbance at the inflow, containing the two frequencies $F_1 = 0.8 \times 10^{-4}$ and $F_2 = F_1/2$. The nondimensional frequency F is defined as $F = 2\pi f\nu/U_{\infty_i}^2$, where f is the dimensional frequency in cycles per second, and ν is the kinematic viscosity. The fundamental frequency F_1 corresponds to $f = 1750$ cps. The fundamental and its subharmonic are turned on for the duration of one cycle of the subharmonic, forming a wave packet that grows and decays as it convects over the curved surface.

The character of the wave packet is illustrated by the instantaneous total vorticity plots shown in Fig. 4 in terms of nondimensional time tU_∞/L, where L is a unit length. For all of the frames a constant range of the vorticity level is plotted. The total vorticity is initially amplified on the flat portion. Additional amplification comes on the concave curvature due to the unfavorable pressure gradient, while farther downstream, the favorable pressure gradient results in a reduction of the total vorticity. The figure distinctively shows that as the disturbance passes over the concave portion drastic changes occur in bandwidth, showing that the favorable pressure gradient stabilizes certain components, as if the flow has passed through a bandpass filter. This phenomenon is strongly dependent on the geometry of the curvature inducing the pressure gradient.

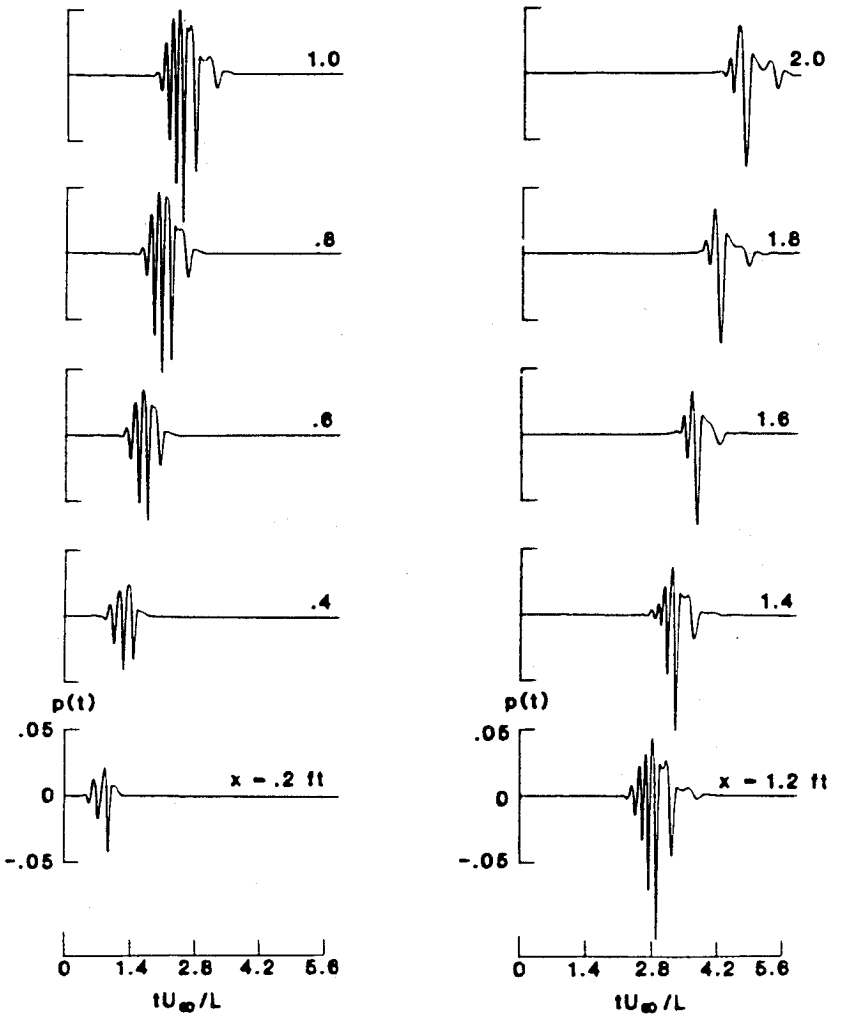

Fig. 5 Wall pressure perturbation along the surface.

B. Acoustic Radiation

The unsteady results presented earlier indicate that the stability of the flow is strongly dependent on the surface geometry. Acoustic radiations, which depend on the rate of changes within the flow, are present even when the flow is being stabilized. In addition, acoustic radiations are known to produce instability that may lead to transition.

Figure 5 shows the wall-pressure perturbation computed from the Navier-Stokes equations that is used as a boundary condition to calculate the far-field sound. The amplitude variation with time has a behavior similar to that of the mass flux variation.[17]

Here, we show results of the calculated acoustic field obtained from the solution of the linearized Euler equations. Figures 6–9 show the pressure perturbation evaluated at 2-, 5-, 7-, and 11-ft radii from the center of the sources over a 180-deg arch. Results show that at 90 deg the rate of decay of the acoustic intensity is exponential in the near field and becomes algebraic in the far field (see Ref. 17 for more details). Similar behavior is also seen in the upstream and downstream quadrants with different rates of decay for the near field.

Figures 6–9 distinctively show strong beaming of the pressure perturbation at $\phi = 60$ deg in the upstream direction. In addition, a weaker beaming is shown downstream at an angle $\phi = 135$ deg. This directivity pattern indicates the dipole character of the source field. Similar findings were reported by Crighton and Huerre[7] and Haj-Hariri and Akylas[8] for the radiation field resulting from the evolution of disturbances on a flat surface. However, in the present study the coupling between the instability wave packet and the geometrical changes of the wall is the main acoustic source, which does not depend on the artificial manner in which the wave packet is started, as indicated by Ref. 8. When considering the sound radiation by flow over a forward-facing step, Howe[18] arrived at the same conclusion that the radiation is of dipole type and preferentially in the upstream and downstream directions. This indicates that the directivity characteristics observed in the present study are not dependent on the surface geometry.

The pressure perturbations shown in Figs. 6–9 exhibit high initial amplitude and a low-frequency peak followed by a high-frequency response. The initial part is the remnant of the input packet. At $\phi = 60$ deg, the amplification of the high-frequency pressure response is significantly higher compared with all other angles.

Figures 6–9 also show the influence of the convection on the propagation of the acoustic waves. This can be observed from the change in the time delay of the initial perturbation at different angular positions; except for $\phi = 90$ deg, the time delay is only influenced by the far-field position.

C. Control of the Far-Field Sound

The control model discussed in the subsection on active sound suppression is applied to the far field, with different settings for the control system to adjust the amplitude of the interference signal at different angles. Acoustic signals at a 7-ft radius from the source are used to control the arriving signals at an 11-ft radius.

A finite number of detectors (microphones) are distributed at a 7-ft arch (every 15 deg) to detect the incoming pressure signals. These signals are fed separately to different filters and then to controllers (speakers) placed at an 11-ft radius. The

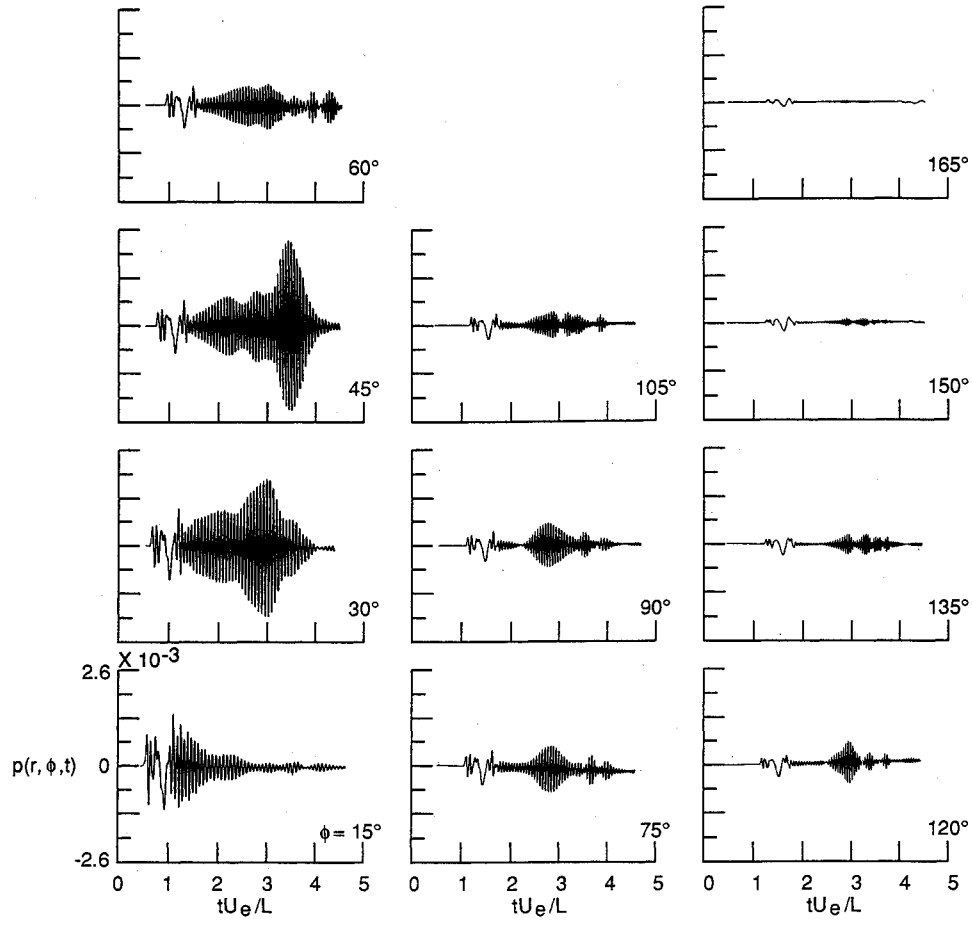

Fig. 6 Free-field pressure perturbation over a 2-ft-radius arch.

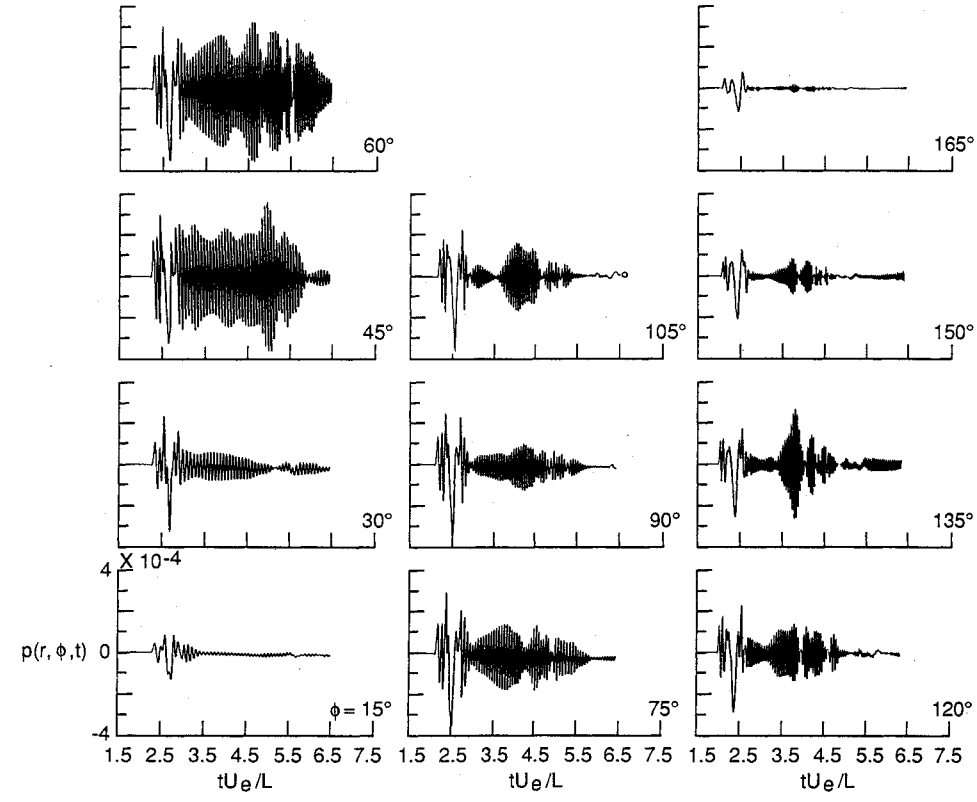

Fig. 7 Free-field pressure perturbation over a 5-ft-radius arch.

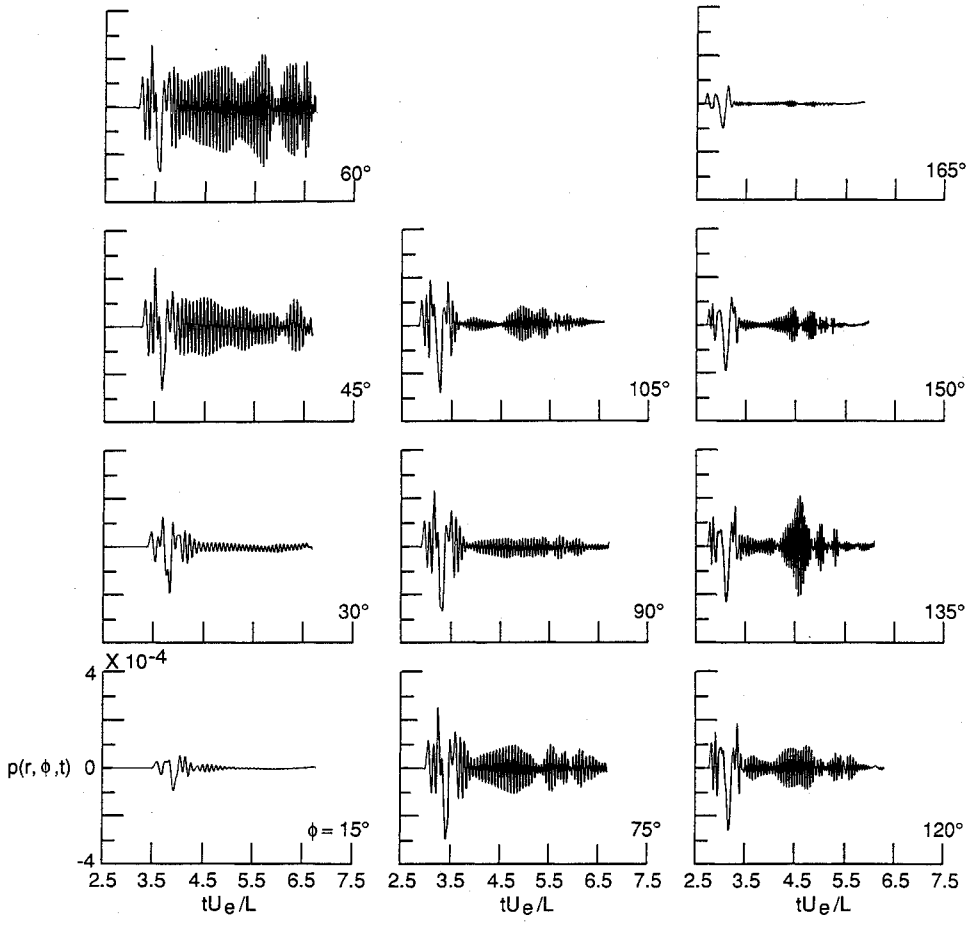

Fig. 8 Free-field pressure perturbation over a 7-ft-radius arch.

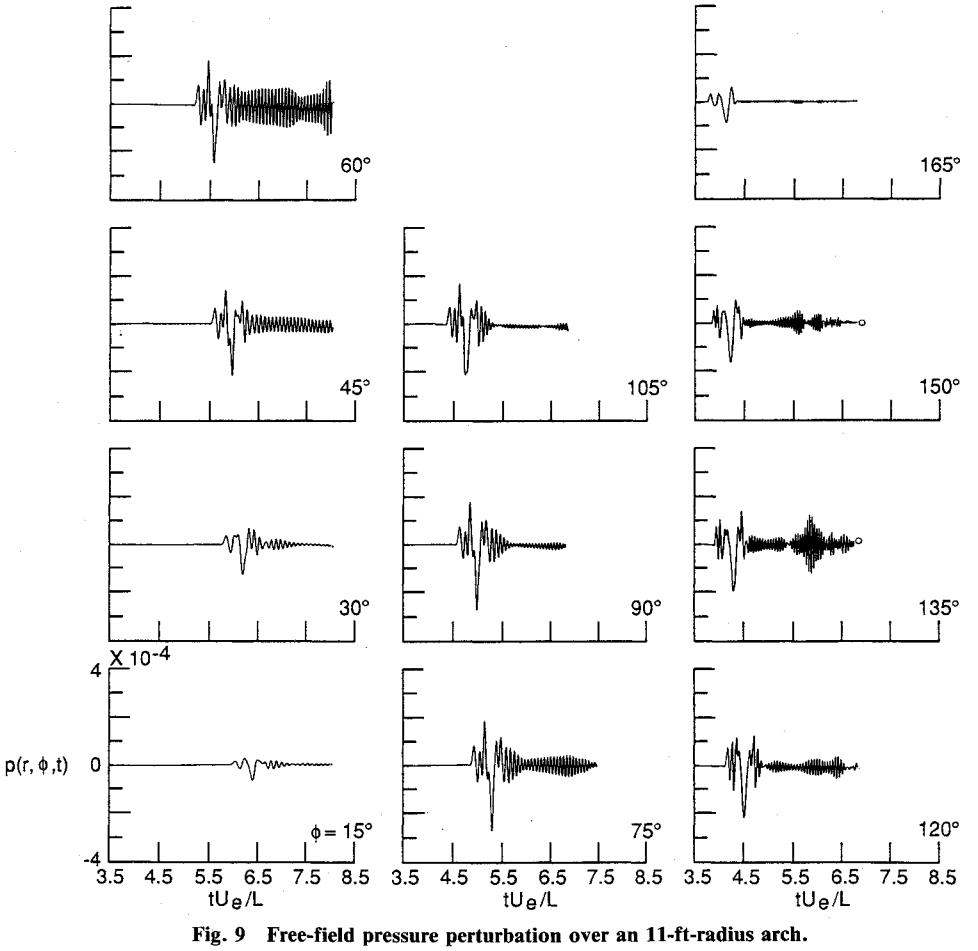

Fig. 9 Free-field pressure perturbation over an 11-ft-radius arch.

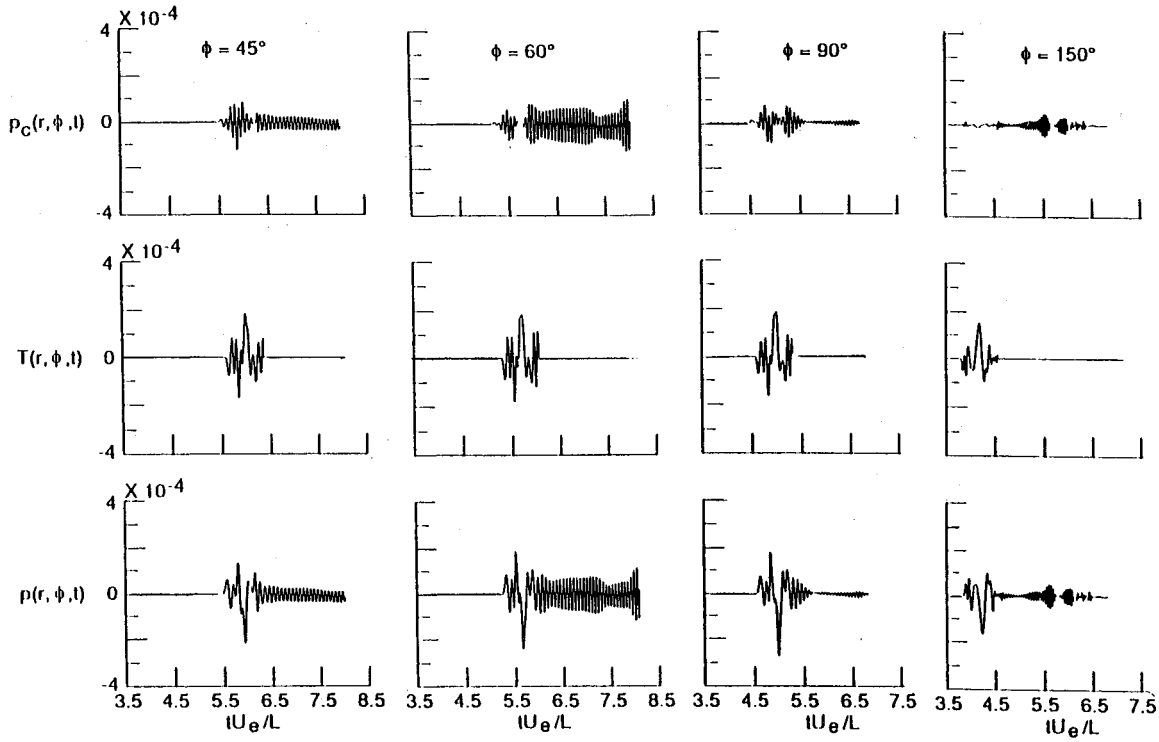

Fig. 10 Reference pressure signal $p(r,\phi,t)$ at a 7-ft radius, interference signal $T(\phi,t)$, and controlled pressure signal $p_c(r,\phi,t)$ at an 11-ft-radius at $\phi = 45$, 60, 90, and 150 deg.

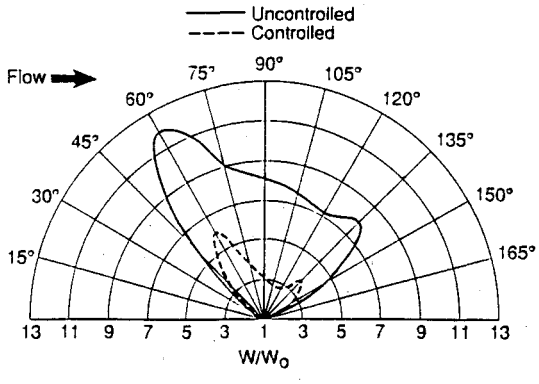

Fig. 11 Uncontrolled and controlled acoustic intensity at an 11-ft radius.

filters compensate for the amplitudes and bandwidths of the arriving signals, and shift them to new initial times determined by the events at 11 ft, where detectors are placed to trigger the controllers. The resulting output from the controllers produces an interference field that attenuates or cancels the direct field.

The control results are shown in Fig. 10 for $\phi = 45$, 60, 90, and 150 deg. The figure contains the reference signal $p(r,\phi,t)$ at a 7-ft radius, the interference signal $T(\phi,t)$, and the resulting attenuated pressure signal $p_c(r,\phi,t)$ at an 11-ft radius. The filters chosen have limited bandwidth, passing only the initial low-frequency, high-amplitude part of the radiation field. Therefore, only the low-frequency part of the pressure signal at 11 ft is attenuated. The effectiveness of the control can be observed by comparing $p_c(r,\phi,t)$ in Fig. 10 with the signal at 11 ft in Fig. 9 at the corresponding angle.

The effectiveness of the control can distinctively be shown from the acoustic intensity plot in Fig. 11. The figure shows a reduction of the normalized acoustic intensity W at an 11-ft radius from uncontrolled to controlled conditions. This reduction corresponds to a 6-dB change in amplitude. The figure clearly shows the directivity character of the far-field sound. The intensity peaks upstream at $\phi = 60$ deg and downstream at $\phi = 135$ deg with an upstream dominating level. The acoustic control can be further improved to account for the high-frequency radiation that dominates at $\phi = 60$ deg with respect to all other angles.

IV. Concluding Remarks

In this paper we have studied numerically the two-dimensional evolution and control of the acoustic pressure in the far field resulting from the growth and decay of a wave packet in an unstable boundary layer over a concave-convex curvature at a freestream Mach number of 0.4.

The behavior of the wave packet in the boundary layer is investigated using direct computations of Navier-Stokes equations. It is shown that the wave packet grows over the concave portion of the surface with a bandwidth broadening due to the destabilizing mean pressure gradient.

The resulting acoustic radiation is computed by solving the linearized Euler equations using the pressure fluctuations computed from the Navier-Stokes equation as a time-dependent boundary condition. Inviscid results show that the pressure disturbance decays exponentially away from the wall in the near field, with the decay becoming algebraic in the far field. In both the near and far fields a directivity pattern appears to point upstream and exhibit an enhanced amplification in time, a behavior that is consistent with previous findings.[7,8]

Active sound control is accomplished by activating a secondary perturbation designed to destructively interfere with the outgoing wave field. Because of the inhomogeneity of the sources and the resulting radiating field, different settings of the control system are applied at different angles to control the acoustic radiation in the far field. By applying this control approach at finite angles (every 15 deg) along the 180-deg arch, it was possible to reduce the amplitude of the acoustic radiation by 6 dB. This concept of active control may be applicable to wind-tunnel contraction, where noise radiated from the concave-convex surface is known to exist.

The effectiveness of the control system can be enhanced by considering the three dimensionality of the acoustic field. In this case a line source or the full three-dimensional source field

must be calculated. This point is worth a forthcoming separate investigation.

Acknowledgment

N. M. El-Hady acknowledges the support of NASA Langley Research Center under contract 18599.

References

[1]Maestrello, L., Bayliss, A., Parikh, P., and Turkel, E., "Active Control of Compressible Flows Over a Curved Surface," *SAE 1985 Transactions,* Vol. 94, Sec. 6, 1986, pp. 664–673.

[2]Maestrello, L., Bayliss, A., Parikh, P., and Turkel, E., "Stability and Control of Compressible Flows Over a Surface with Concave-Convex Curvature," International Council of the Astronautical Sciences Rept. 86-48, July 1986.

[3]Dines, P. J., "Active Control of Flame Noise," Ph.D. Dissertation, Cambridge University, Cambridge, UK, 1984.

[4]Ffowcs Williams, J. E., and Huang, X. Y., "Active Stabilization of Compressor Surge," *Journal of Fluid Mechanics,* 1989 (to be published).

[5]Maestrello, L., "Active Transition Fixing and Control of the Boundary Layer in Air," *AIAA Journal,* Vol. 24, No. 10, 1986, pp. 1577–1581.

[6]Crighton, D. G., and Huerre, P., "Model Problems for the Generation of Superdirective Acoustic Fields by Wave Packets in Shear Layers," AIAA Paper 84-2295, Oct. 1984.

[7]Haj-Hariri, H., and Akylas, T. R., "Sound Radiation by Instability Wavepackets in a Boundary Layer," *Studies in Applied Mathematics,* Vol. 75, 1986, pp. 57–76.

[8]Ffowcs Williams, J. E., "Control of Unsteady Flows," AIAA Paper 89-0990, March 1989.

[9]Bayliss, A., Parikh, P., Maestrello, L., and Turkel, E., "A Fourth-Order Scheme for the Unsteady Compressible Navier-Stokes Equations," AIAA Paper 85-1694, July 1985.

[10]El-Hady, N. M., "HADY-I, a FORTRAN Program for the Compressible Stability Analysis of Three-Dimensional Boundary Layers," NASA CR-3467, Sept. 1981.

[11]Lighthill, M. J., "On Sound Generated Aerodynamically, I: General Theory," *Proceedings of the Royal Society of London, Series A,* Vol. 221, March 1952, pp. 564–587.

[12]Howe, M. S., "Contributions to the Theory of Aerodynamic Sound with Application to Excess Jet Noise and the Theory of the Flute," *Journal of Fluid Mechanics,* Vol. 71, Pt. 4, 1975, pp. 625–673.

[13]Hardin, J. C., and Lamkin, S. L., "Aeroacoustic Interaction of a Distributed Vortex with a Lifting Joukoweski Airfoil," AIAA Paper 84-2287, 1984.

[14]Farassat, F., "Discontinuity in Aerodynamics and Acoustics—Concept and Application of Generalized Derivatives," *Journal of Sound and Vibration,* Vol. 55, No. 2, 1977, pp. 165–193.

[15]Bayliss, A., Jordan, K. E., Lemesurier, B. J., and Turkel, E., "A Fourth-Order Accurate Finite Difference Scheme for the Computation of Elastic Waves," *Bulletin of Seismological Society of America,* Vol. 76, No. 4, 1986, pp. 1115–1132.

[16]Smith, W. D., "A Non-Reflecting Plane Boundary Condition for Wave Propagation Problem," *Journal of Computational Physics,* Vol. 15, Feb. 1974, pp. 492–503.

[17]Maestrello, L., Parikh, P., and Bayliss, A., "Instability and Sound Emission from a Flow Over a Curved Surface," *Journal of Vibration, Stress, and Reliability in Design,* Vol. 110, Oct. 1988, pp. 538–544.

[18]Howe, M. S., "Sound Produced by Turbulent Boundary Layer Flow Over a Finite Region of Wall Roughness and Over a Forward Facing Step," *Journal of Fluids and Structures,* Vol. 3, Jan. 1989, pp. 83–96.